Aquatic Sciences 54, 3/4, 1992

1015–1621/92/040179–01 $1.50+0.20/0

Editorial

All of the papers in this issue of Aquatic Sciences were presented at a symposium held in Lugano, Switzerland, 5–7 November, 1990. The symposium, "Limnological Aspects and Management of Lago di Lugano", was directed at promoting cooperation between limnologists and public bodies in the restoration of the Lago di Lugano. To this end the researchers involved in studying the lake over the last few years were invited to present the existing situation. The high quality of the numerous papers presented at the symposium confirmed that the Lago di Lugano is one of the best-studied lakes in recent times. This is due to several activities; the "Commissione Internazionale per la Protezione delle Acque Italo-Svizzere" has promoted limnological studies since 1978; for the last 12 years these studies have been the responsibility of the Laboratorio Studi Ambientali, while other scientists have studied the sediments and the fish fauna of the lake. Limnological knowledge of the lake has also been extended by the scientific project "Endoceresio 1989", sponsored by the Credit Union Bank of Lugano.

The papers in this issue show that Lago di Lugano is still eutrophic, despite the large-scale recovery measures applied over the last 20 years. The results confirm that only the orchestrated contribution of different scientists working in the fields of physics, chemistry, biology and geology can lead to a better knowledge of the limnological processes in the lake. Questions were raised about the exchange water-sediments and the meromixis stability observed in the northern basin. Despite the high level of limnological knowledge attained, the symposium highlighted the need for coordinated projects between research institutes working in different fields. Such collaboration would enable the problems aired at the symposium to be solved. The contribution of scientists is crucial to the course that the administrators decide to take as far as recovery measures are concerned. The final conclusion of the symposium was that the lake must be protected to guarantee its use as a drinking water supply and as a recreational and natural resource.

The "Limnological Aspects and Managements of Lago di Lugano" symposium was promoted by the Swiss Limnological Society and organised by the Laboratorio Studi Ambientali and the Laboratorio di Fisica Terrestre of Canton Ticino. Special thanks are due to the Credit Union Bank of Lugano and to the Lugano City Council for their support.

Alberto Barbieri and Bruno Polli
June 10, 1992

Aquatic Sciences 54, 3/4, 1992

1015–1621/92/040181–03 $1.50 + 0.20/0

Description of Lake Lugano

Alberto Barbieri and Bruno Polli

Laboratorio Studi Ambientali, Sezione Protezione Aria e Acqua, Dipartimento del Territorio, 6500 Bellinzona, Canton Ticino, Switzerland

Border area between Switzerland (Cantone Ticino) and Italy (Regione Lombardia) 46°00′N, 3°30′E; 271 m above sea level.

Description

The Lago di Lugano lies in a valley which resulted from a fluvial erosion in a tertiary (messinian) canyon which underwent a strong morphological overprint during the pleistocene Alpine glaciations.

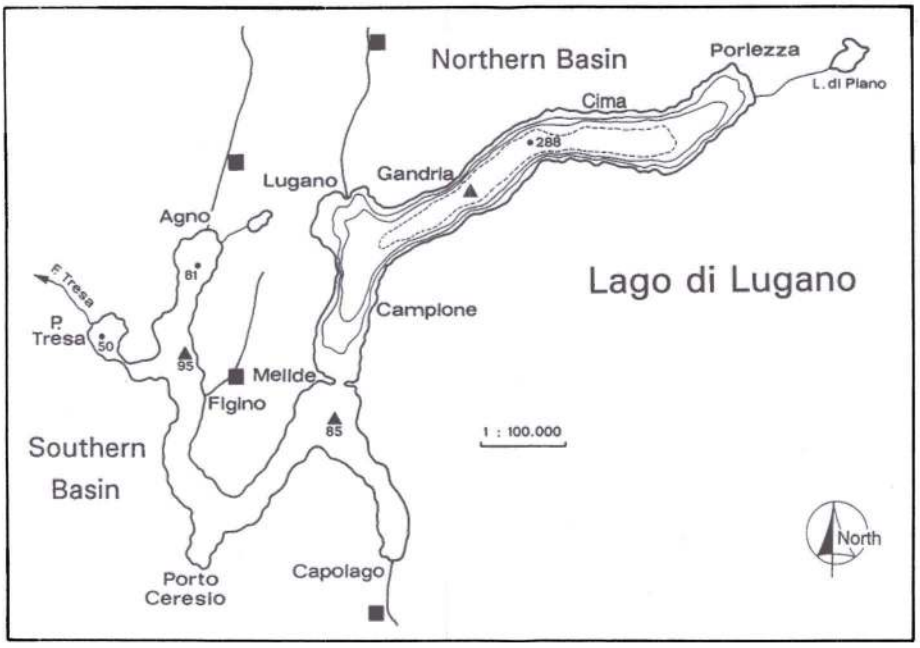

Figure 1. Map of Lago di Lugano. ▲ Principal sampling stations for the research program of the Commissione Internazionale per la Protezione delle Acque Italo-Svizzere. ■ Wastewater treatment plants

Table 1. Morphological and hydrological characteristic of Lago di Lugano

basin		Northern	Southern
Drainage basin (lake excluded)	km^2	269.7	587.5
Lake area	km^2	27.5	20.3
Maximum depth	m	288	95
Volume	km^3	4.69	1.14
Mean depth	m	171	55
Output volume	km^3 a	0.38	0.77
Mean residence time	a	12.3	1.4

Table 2. Volume and areas of the two basins of Lago di Lugano

Northern depth m	area km^2	volume km^3	Southern depth m	area km^2	volume km^3
0	27.5		0	20.3	
5	27.0	0.136	5	19.2	0.098
10	26.6	0.270	10	18.7	0.193
15	26.2	0.402	15	18.1	0.285
20	25.8	0.532	20	17.5	0.374
30	25.1	0.786	30	16.4	0.543
50	23.6	1.273	50	14.1	0.848
100	19.7	2.353	93	1.2	1.137
150	16.0	3.244			
200	12.8	3.963			
250	7.9	4.476			
286	1.9	4.682			

Table 3. Climatic data at Lugano, 1951–1980

	Jan	Feb	Mar	Apr	May	Jun	Jul	Aug	Sep	Oct	Nov	Dec	Annual
Mean temp [°C]	2.4	4.1	7.5	11.4	15.5	19.0	21.4	20.6	17.5	12.4	7.2	3.5	11.9
Precipitation [mm]	77	84	112	146	179	202	158	185	162	170	156	78	1709

It is divided into two parts by a morainic front on which an artificial damn was built to connect the two shores. This resulted in the lake being split into two basins with specific characteristics (Fig. 1; Tab. 1; Tab. 2). The northern basin is deep and its catchment area is limited with respect to the volume of the lake, causing a long mean residence time of the water (12.3 a). The eutrophication process which started in the second half of this century has caused the meromictic behaviour of this basin, thereby making renewal of the water more difficult.

The southern basin is less deep, it sides are less steep (Tab. 2) and its behaviour is holomictic, with a short residence time of the water (1.4 a).

The insubric climate (Tab. 3) and the morphology of the land, typically prealpine, make the tributaries of the lake torrential even though they are small.

Table 4. Equivalent inhabitants (EI) in the watershed of Lago di Lugano, 1990

	resident EI	discharging EI	treated	untreated
northern basin	200000		17%	83%
southern basin	100000		80%	20%

Most of the catchment area, and in particular the riverain territory, has seen a marked demographic development caused by its attractiveness as a residential, industrial and touristic area.

With the construction of sewage treatment plants, which include mechanical, biological and chemical process in the form of phosphorus flocculation for about 67% of the wastewater in the catchment area, the loading of organic material and phosphorus compounds has been reduced and the trophic state has tended toward at lower level. Tab. 4 shows that the loading resulting from 140000 equivalent inhabitants residing in the catchment area of the northern basin has been transferred to the southern basin through the water purification plant near Agno (Fig. 1). This, together with the geomorphological and limnological peculiarities of the two basins, explains their different trophic evolution.

Aquatic Sciences 54, 3/4, 1992

1015–1621/92/040205–14 $1.50 + 0.20/0

Density Structure and Tritium-Helium Age of Deep Hypolimnetic Water in the Northern Basin of Lake Lugano

A. Wüest [1], W. Aeschbach-Hertig [1], H. Baur [2], M. Hofer [1], R. Kipfer [1] and M. Schurter [1]

[1] Environmental Physics, Institute for Aquatic Sciences and Water Pollution Control, ETH-Zürich, c/o EAWAG, CH-8600 Dübendorf, Switzerland
[2] Isotope Geochmistry, NO C61, ETH-Zürich, CH-8092 Zürich, Switzerland

Key words: Biogenic stagnation, vertical mixing, tritium-helium age, double diffusion; boundary mixing, deep lakes, Lake Lugano (Lago di Lugano).

ABSTRACT

Long-term stratification of the deep hypolimnetic waters of the northern basin of Lake Lugano (Lago di Lugano) has resulted in a lack of deep-water renewal which has persisted for decades. Tritium-helium age measurements reveal that deep water has not been in contact with the atmosphere since the 1960s. Higher primary production associated with the significant increase in phosphorus concentration which occurred at this time resulted in greater autochthonous gross sedimentation rates, increasing the rate of mineralization and, consequently, the rate of release of dissolved solids (mainly HCO_3^- and Ca^{2+}) into the deep hypolimnion. This gave rise to an intensification of the stratification and to a consequent reduction in the vertical exchange of hypolimnetic water layers. Today, the density stabilizing effect of ion release due to mineralization in the deep water is four to five times greater than the destabilizing effect of the geothermal heat flux from the earth's interior. It is known from laboratory experiments that such small density gradient ratios are likely to give rise to double-diffusive instabilities. However, even rudimentary mass balance calculations of biogeochemical components indicate that shear-induced turbulence, most likely generated by bottom currents, mixes far more efficiently than double diffusion. In the future, the biogenic density stratification is likely to persist in the deep water, unless the upward ion flux, driven by primary production, decreases by a factor of four to five.

1. Introduction

Monthly profiles of temperature and electrical conductivity (CTD) measured during the last few years in the deep water of the northern basin of Lake Lugano have been found to vary only slightly (LSA, 1990; Barbieri and Mosello, this issue). Vertical thermal convection accompanied by winter cooling obviously did not reach the deepest point of the lake (288 m). It is tempting to assume that the lack of deep convection is associated with low wind activity, resulting from the sheltering effect of the surrounding high mountains (Barbieri and Polli, this issue). Low wind activity cannot, however, be the only reason for this phenomenon, since one would expect

deep mixing at least sporadically during cold periods in a purely thermally stratified temperate lake. In the northern basin of Lake Lugano, however, the incomplete mixing is not only the result of low wind activity, but is also a consequence of long-term lake eutrophication: mineralization of biomass in the hypolimnion leads to an accumulation of dissolved solids in the deep waters and thus to a chemically-induced permanent density stratification (Joller, 1985). As a result, the oxygen supply to the deep waters has been insufficient to prevent the occurrence of anoxia in the deep hypolimnion since the 1960s (Barbieri and Mosello, this issue).

In contrast to the mineralization processes, the geothermal heat flux from the sediments reduces the bottom water density, thus tending to stimulate vertical mixing. The two components of the vertical density gradients associated with dissolved solids and temperature thus have opposite signs. At least once in the recent past it has been observed that the positive stability associated with the dissolved solids concentration gradient was only 80% greater than the negative stability associated with the temperature profile (Karagounis, 1992). In this so-called "diffusive regime", small scale (dm to m) vertical instabilities in the water column may occur as a result of double diffusion. This process, uncommon in freshwater lakes, could enhance vertical exchange and partially nullify the effect of the stratification. The magnitude of the vertical fluxes involved are of prime interest with respect to water quality, since the deep hypolimnion of Lake Lugano acts as a large phosphorus reservoir (Barbieri and Mosello, this issue).

In order to understand this particular mixing regime, we determined the vertical fine-scale density structure of the deep hypolimnion (Section 2) and calculated the tritium-helium age of the water column (Section 3). ("Deep hypolimnion" refers here to the water body below 150 m depth.) By assuming stationary conditions in the deep hypolimnion, we calculated vertical mixing rates which are shown to be consistent

Table List of symbols

$A(z)$	m^2	Cross-sectional lake area as a function of depth z
α	K^{-1}	Thermal expansivity of water
c_p	$4200\,J\,kg^{-1}\,K^{-1}$	Specific heat
F_{geo}	$W\,m^{-2}$	Geothermal heat flux
F_{sed}	$kg\,m^{-2}\,s^{-1}$	Vertical mass flux of dissolved solids
g	$9.81\,m\,s^{-2}$	Acceleration of gravity
[^{3}H]	m^{-3} or TU	Tritium concentration
[^{3}He]	m^{-3}	Helium-3 concentration
γ_ϱ	$(\mu S\,cm^{-1})^{-1}$	Relative change of density per unit electrical conductiviy
γ_s	$‰(\mu S\,cm^{-1})^{-1}$	"Salinity" per unit electrical conductivity
K_d	$m^2\,s^{-1}$	Vertical (diapycnal) eddy diffusivity
κ_{20}	$\mu S\,cm^{-1}$	Electrical conductivity at $T = 20\,°C$
N	s^{-1}	Stability frequency
R_ϱ	–	Density gradient ratio
ϱ	$kg\,m^{-3}$	Density
S	‰	"Salinity"
t, τ	s	Time
T, T_{abs}	°C, K	Temperature, absolute Temperature
u_{1m}	$m\,s^{-1}$	Current velocity 1 m from the lake bottom
z	m	Vertical coordinate (positive upwards)

with the observed biogeochemical gradients and with the helium-3 and tritium content of the deep hypolimnion (Section 4). The data set discussed in this paper was obtained on May 15/16, 1990. It comprises five fine-scale CTD profiles taken along the mid-lake axis (Fig. 1 in Barbieri and Polli, this issue), one profile of tritium-helium samples (15 m vertical resolution) and three samples of dissolved solids.

2. Density structure

a) Temperature profile and geothermal heat flux

The dominant feature of the temperature profiles, viz. the inverse gradients in the hypolimnion, is illustrated in Fig. 1. The two examples of temperature profiles shown (from February 1988 and May 1990) illustrate the temperature regime in the hypolimnion. Above the deep hypolimnion (< 150 m depth), the temperature is obviously subject to transient changes dependent on rates of surface heating/cooling and vertical mixing. In this region of the lake, surface cooling can produce very distinct temperature inversions (e.g. in February 1988: Fig. 1), giving rise to a situation in which double diffusion is likely to occur. This will be discussed in Section 4. (During the warm winters of 88/89 and 89/90, the maximum depth of winter

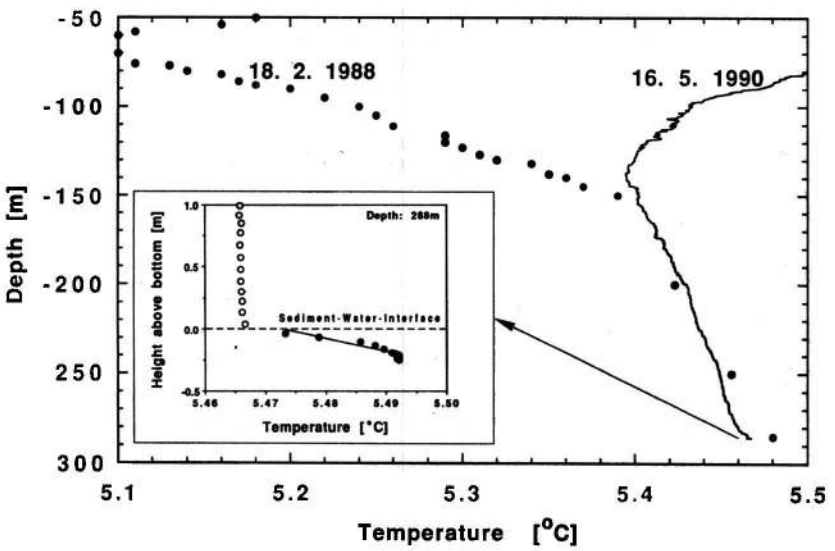

Figure 1. Temperature profiles measured on 16 May 1990 ($\approx$ 3 cm vertical resolution) (line) and on 18 February 1988 (LSA, 1990) (dots). Details of the fine-structure profile are shown in Fig. 7 (close to the bottom) and in Wüest et al. (1990) (spiky structure between 100 and 125 m).
Inset: The geothermal heat flux from the earth's interior leads to a temperature gradient of $\partial T/\partial z \approx 0.10\,\mathrm{K\,m^{-1}}$ in the upper sediment layer. The corresponding molecular heat flux $D_T^{Sed} \cdot \partial T/\partial z \approx 0.086\,\mathrm{W\,m^{-2}}$ (with the thermal conductivity of the sediment $D_T^{Sed} \approx 0.86\,\mathrm{W\,m^{-1}K^{-1}}$) is close to the mean geothermal heat flux of $0.097\,\mathrm{W\,m^{-2}}$ measured by Finckh (1981)

cooling was far less than 150 m (LSA, 1990), and consequently, the temperature above 150 m depth has increased since February 1988.)

In the deep hypolimnion, however, according to the monthly profiles (LSA, 1990), the inverse vertical temperature gradient is persistent. On May 15, 1990, the vertical gradient was almost constant at $-4.5 \cdot 10^{-4}\,\mathrm{K \cdot m^{-1}}$ (Fig. 1). As the permanent gradient is so small, adiabatic compression may be considered as a possible reason for the temperature increase at greater depth. However, the adiabatic lapse rate of nearly fresh water at 5.4 °C,

$$\left.\frac{\partial T}{\partial z}\right|_{\mathrm{ad}} = -\frac{g\alpha T_{\mathrm{abs}}}{c_{\mathrm{p}}} = -0.15 \cdot 10^{-4}\,\mathrm{K \cdot m} \tag{1}$$

(for symbols see Table) is as much as 30 times smaller than the vertical temperature gradient and may consequently be neglected. The persistent gradient therefore results from a balance between the geothermal heat influx $F_{\mathrm{geo}} = (97 \pm 10) \cdot 10^{-3}\,\mathrm{W\,m^{-2}}$ (Finckh, 1981), and the outflux due to vertical mixing. The time scale required to establish such a temperature inversion depends on the heating rate

$$\frac{\partial \mathrm{T}}{\partial t}(z) = \frac{\partial}{\partial z}\left(K_{\mathrm{d}}\frac{\partial T}{\partial z}\right) + \frac{1}{\varrho c_{\mathrm{p}} A(z)}\frac{\partial A(z)}{\partial z} F_{\mathrm{geo}}, \qquad [\mathrm{K\,s^{-1}}] \tag{2}$$

which is a function of the morphometry, $A(z)$, and the vertical diffusivity, K_{d}. For the above-mentioned geothermal heat flux, at least several years (≈ 6 yr) are required to build up the observed temperature inversion in the deep hypolimnion. This lower limit of the time scale is obtained by neglecting vertical heat exchange ($K_{\mathrm{d}} = 0$) in Eq. (2). Since vertical small-scale turbulent mixing acts of course to increase this time scale, we can conclude that it is the absence of deep convective mixing over a period of years to decades which has allowed the geothermal heat flux to build up the inverse temperature gradient.

b) Dissolved solids

The fine-scale distribution of dissolved solids is measured indirectly in terms of electrical conductivity. In contrast to the ocean, the relationship between "salinity" (defined here as the mass of dissolved ions per unit mass of lake water) and electrical conductivity is not unique for lakes and has to be established for each individual case. In general, the electrical conductivity of water, κ_{20} (at $T = 20\,^{\circ}\mathrm{C}$), depends on the concentrations c_{i} of all dissolved ions, i. For dilute solutions, such as lake water, the total expected in situ conductivity is given by the sum of the contributions from the individual species:

$$\kappa_{20}(c_1, \quad , c_{\mathrm{n}}) = \sum_{\mathrm{i}=1}^{\mathrm{n}} f_{\mathrm{i}}(c_1, \quad , c_{\mathrm{n}}) \cdot \lambda_{\mathrm{i}}^{\infty} \cdot c_{\mathrm{i}} \qquad [\mu\mathrm{S\,cm^{-1}}] \tag{3}$$

($\lambda_{\mathrm{i}}^{\infty}$ = equivalent conductance at infinite dilution at 20 °C; f_{i} = reduction coefficient as a function of the total ion concentrations (see appendix)). In the Table in the

appendix, the summation is carried out for samples at three different depths. The agreement of the right-hand side of Eq. (3) with the in situ measured conductivity supports the applicability of Eq. (3). Since the concentration is low and the relative composition does not vary significantly, the ratio of salinity to electrical conductivity, γ_s, is practically constant (see Table in the appendix):

$$\gamma_s = \frac{S}{\kappa_{20}} = 0.89 \cdot 10^{-3} \text{ ‰ } (\mu\text{S cm}^{-1})^{-1} = 0.89 \cdot 10^{-6} (\mu\text{S cm}^{-1})^{-1} \quad (4)$$

The vertical salinity profile is determined by the rate of biodegradation of the sinking particles and the rate of vertical mixing. The main product of the mineralization process is CO_2; consequently, the partial CO_2 pressure increases and the pH decreases, resulting in the dissolution of calcite. At the observed in situ pH of 7.3–8.0 (LSA, 1990), more than 84% of the total dissolved inorganic carbon is in the form of HCO_3^-, which is balanced mainly by Ca^{2+} (both together contribute about 90% to the salinity S: see appendix). As a consequence of these processes, the measured steady-state salinity in the hypolimnion increases monotonically with depth from $S = 0.192$‰ ($\kappa_{20} = 216.6\ \mu\text{S cm}^{-1}$) at 30 m to $S = 0.225$‰ ($\kappa_{20} = 252.5\ \mu\text{S cm}^{-1}$) at the maximum depth (Fig. 2). As in the case of the temperature gradient, the conductivity gradient $\partial\kappa_{20}/\partial z$ in the deep hypolimnion is nearly constant: it takes on the value $-0.072\ \mu\text{S cm}^{-1}\,\text{m}^{-1}$.

c) Stability of the water column and double diffusion

We assume that the density of the deep hypolimnetic water is determined by temperature and dissolved solids only (the error introduced by neglecting SiO_2 is about 1%). Figure 2 shows the vertical density profile calculated as

$$\varrho(T, \kappa_{20}) = \varrho_w(T) \cdot [1 + \gamma_\varrho \kappa_{20}], \qquad [\text{kg m}^{-3}] \quad (5)$$

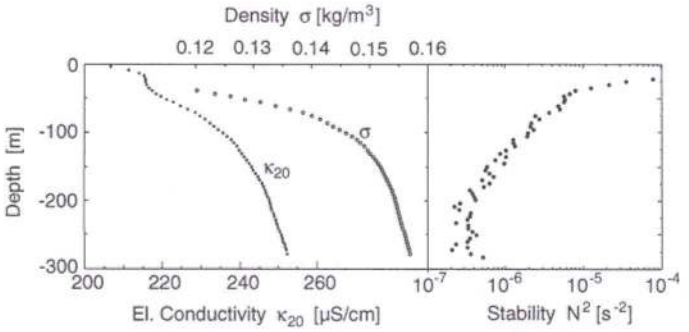

Figure 2. Vertical profiles of conductivity κ_{20}, density (plotted as $\sigma = \varrho - 1000\ \text{kg m}^{-3}$) and stability N^2. One dot represents the average over 5 m and 4 profiles. See Fig. 7 for the fine structure of electrical conductivity and density above the bottom

where $\varrho_w(T)$ expresses the temperature-dependent pure water density and $\gamma_\varrho \kappa_{20}$ the density change due to the dissolved solids found in the lake water. Again, as the composition does not change drastically, the increase in density per unit conductivity is constant for dilute solutions. Using Bührer and Ambühl's (1975) procedure yielded a value of $\gamma_\varrho = 0.70 \cdot 10^{-6}\,(\mu S\,cm^{-1})^{-1}$ for the ionic composition found in the hypolimnion of Lake Lugano.

The static stability of the water column

$$N^2 = -\frac{g}{\varrho}\frac{\partial \varrho}{\partial z} = g\left(\alpha \frac{\partial T}{\partial z} - \gamma_\varrho \frac{\partial \kappa_{20}}{\partial z}\right) \qquad [s^{-2}] \tag{6}$$

(see table for symbols) depends on the water temperature (since $\alpha(T)$ is a function of temperature) as well as on the two gradients $\partial T/\partial z$ and $\partial \kappa_{20}/\partial z$. As shown in Fig. 2, the stability N^2 falls exponentially in the upper hypolimnion (from 50 to 200 m depth) with a depth scale of 53 m and levels off in the lowest 100 m at $N^2_{\text{Bottom}} \approx 3 \cdot 10^{-7}\,s^{-2}$ (Fig. 2).

The relative contribution of the two terms in Eq. (6) to the total stability is commonly expressed by the density gradient ratio

$$R_\varrho = \frac{\gamma_\varrho \partial \kappa_{20}/\partial z}{\alpha\, \partial T/\partial z}, \tag{7}$$

which is plotted in Fig. 3. This plot reveals that salinity dominates stability below 60 m ($|R_\varrho| > 1$). Temperature, however, is stabilizing only above 130 m depth ($R_\varrho < 0$) but destablizing below that depth ($R_\varrho > +1$). Since both gradients in Eq. (7) are almost constant in the deep hypolimnion, the density gradient ratio R_ϱ is consequently also approximately constant there (Fig. 3). The average value of

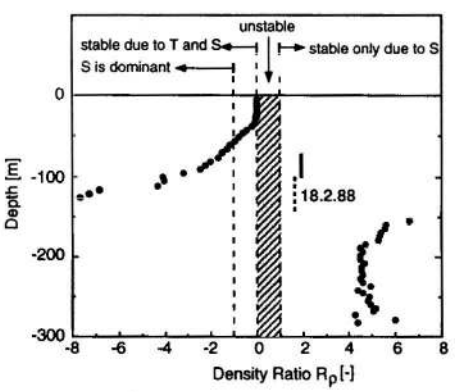

Figure 3. The density gradient ratio R_ϱ, calculated from the 5 m averaged profile measured on May 1990 (Fig. 2), indicates whether temperature T or salinity S is responsible for net stability. According to Eq. (7), salinity destabilizes the water column if $R_\varrho < -1$ or if $R_\varrho > +1$. Consequently, in May 1990, temperature, T, was stabilizing above 60 m and salinity, S, below 60 m depth. Note the low and relatively constant density gradient ration R_ϱ of about 4.5. (On 18 February 1988, R_ϱ attained a value of about 1.8, which is much more favorable to double diffusion: see Fig. 4)

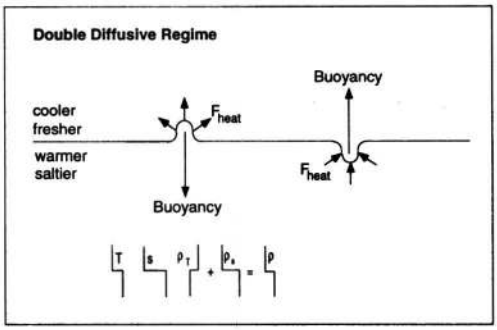

Figure 4. Since the molecular diffusion coefficient of heat, D_T, is far greater than that of salt, D_s, a vertically displaced water parcel can easily cause the exchange of heat (see F_{heat}) without exchanging much salt ($D_T/D_s \approx 150$ for $T = 5\,°C$). As a result, the density of the displaced water parcel is altered in such a way that it is accelerated in the opposite direction beyond its original equilibrium position. There, the same conversion process (with opposite signs) will occur, and this process will be repeated again and again. The accelerated water parcel gives rise to mixing, the rate of which increases as R_ϱ approaches 1. For $1 < R_\varrho < 2$, homogenized layers may be found (Huppert and Turner, 1972; Newman, 1976)

$R_\varrho = 4.5$ implies that salinity stabilizes the water column 4.5 times more than temperature destabilizes the deep water.

Equation (7) clearly indicates that, in the deep water, R_ϱ must always exceed unity ($R_\varrho > 1$), since for the actual signs of the gradients, $N^2 = g \cdot \alpha \cdot \partial T/\partial z \cdot (1 - R_\varrho)$ would become negative (unstable) for $0 < R_\varrho < 1$. Although all values of $R_\varrho > 1$ theoretically imply static stability, R_ϱ can only approach, but never reach unity under conditions found in aquatic systems, since for values of R_ϱ close to unity, instabilities due to double diffusion would occur, as explained in Fig. 4. These instabilities are due to the fact that the molecular diffusion of heat occurs about 150 times faster than that of dissolved solids (Fig. 4). The energy for the local small-scale convections which generate mixing is drawn from the potential energy stored in the stratification.

Low values of R_ϱ favorable to double diffusion will be reached especially during winter in the upper hypolimnion, when surface cooling increases the temperature inversion, as shown in Fig. 1. The February 1988 profile is an example for an unusually low value of R_ϱ, viz. $R_\varrho \approx 1.8$ (Fig. 3). In natural water bodies, values, so close to unity are usually accompanied by a layered profile structure (Turner, 1973; Padman and Dillon, 1987). Section 4 addresses the question of whether fluxes related to double-diffusive mixing represent a relevant contribution to the total flux.

3. Tritium-helium age of the water column

Super-heavy hydrogen, tritium ^3H, is washed from the atmosphere into lakes by rainfall and subsequent drainage. As tritium is radioactive and disintegrates to ^3He as follows:

$$^3H \left(\overset{\beta^-}{\rightarrow}\right) {}^3He \qquad \tau_{1/2} = 12.51 \text{ yr},$$

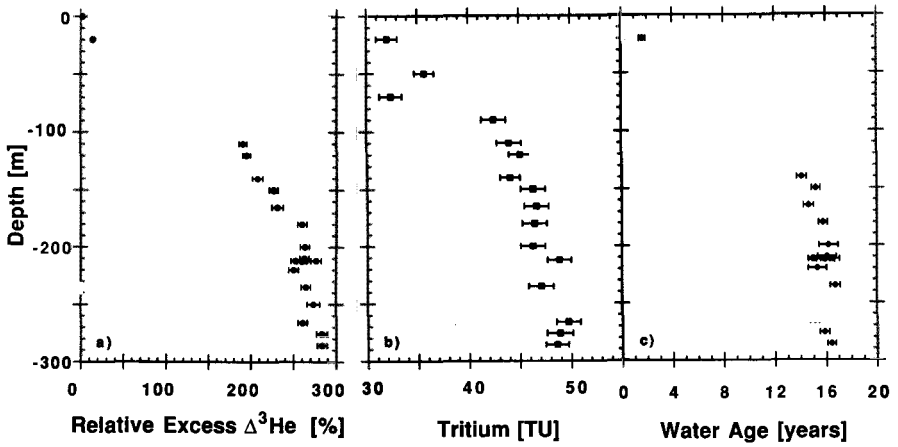

Figure 5. a) Relative ^{3}He excess. (Δ^3He is defined as the relative difference between the observed ^{3}He concentration [^{3}He^{obs}] and the saturation concentration [^{3}He^{sat}], determined by the atmospheric pressure at the lake surface (270 m asl), i.e. $\Delta^3\text{He}[\%] = \{([^3\text{He}^{obs}]/[^3\text{He}^{sat}]) - 1\} \cdot 100\%$). b) Tritium concentration (1 TU corresponds to a tritium/hydrogen ratio of 10^{-18}). c) Tritium-helium age calculated by Eq. (8)

the ^{3}H and ^{3}He concentrations ([^{3}H] and [^{3}He], respectively) of a closed water system can be used to determine the tritium-helium water age τ, defined as the time interval since the last gas equilibration with the atmosphere. If water is no longer in contact with the atmosphere, [^{3}He] increases and [^{3}H] declines. This increase in [^{3}He] leads to an excess concentration, [$^3\text{He}_{ex}$], which expresses the difference between [^{3}He] as measured in situ and the atmospheric saturation value given by Henry's Law. In this case, the tritium-helium age τ depends only on the actual values of [$^3\text{He}_{ex}$] and [^{3}H] and is given by (Torgersen et al. 1979) as:

$$\frac{\tau_{1/2}}{\ln(2)} \cdot \ln\left(1 + \frac{[^3\text{He}_{ex}]}{[^3\text{H}]}\right) \qquad [\text{yr}] \tag{8}$$

Based on measured values of [$^3\text{He}_{ex}$] (Fig. 5a) and [^{3}H] (Fig. 5b), the tritium-helium age profile was estimated using Eq. (8) (Fig. 5c). The age of about 15 years thus obtained (Fig. 5c) has to be regarded as a minimum, since the deep water is not a closed system and ^{3}He and ^{3}H both undergo mixing. As a result of vertical mixing and the presently existing vertical gradients (Fig. 5) both isotopes are now exported from the deep water body. The tritium-helium water age is affected by the mixing of the two isotopes in opposite ways. Eq. (8) indicates that while ^{3}He loss decreases the tritium-helium water age, ^{3}H loss increases it. Given the present vertical distributions, the effect of ^{3}He loss is much the stronger, resulting in a systematic underestimate of water age. For a vertical diffusivity of $3 \cdot 10^{-5}$ m^2 s^{-1} in 150 m depth (see next Section), the water age increases annually only by about six months. The high tritium concentration of the deep water ($\approx$ 48 TU; 1 TU $\equiv [^3\text{H}]/[^1\text{H}] \cdot 10^{18}$), which amounts to twice the present concentration in

rainwater, is a strong hint that the main tritium input occurred in the early 1960s when the atmospheric tritium content was very high due to nuclear bomb testing. Calculations using a one dimensional vertical diffusion/reaction model (Ulrich, 1991) based on the historical record of tritium concentrations in rainwater (Weiss and Roether, 1980; KUeR, 1991) as input revealed that the assumption of "no deep water convection since the main tritium input in 1963" is consistent with the present profile.

4. Density structure in relation to deep water mixing

a) Steady state vertical mixing

In the following, we assume that temperature and salinity profiles are at steady state in the quasi-permanently stratified deep hypolimnetic water. This assumption is justified since the time scale for build-up of the inverse temperature gradient (≈ 6 years, Eq. (2)) is significantly shorter than the tritium-helium water age. We shall now discuss both vertical mixing processes, i.e. small-scale turbulence and double diffusion.

If vertical mixing is due to small-scale turbulence, vertical fluxes can be described by Fickian diffusion with a suitable value for the eddy diffusivity K_d. At steady state, K_d is obtained by the flux balance between the geothermal heat flux into, and the turbulent flux out of, the deep water. By assuming the geothermal heat flux to enter vertically into the lake water, we can determine the vertical diffusivity using

$$K_d(z) = -\frac{F_{geo}}{\varrho c_p \partial T/\partial z}(z), \qquad [m^2\,s^{-1}] \tag{9}$$

as shown in Fig. 6 for $F_{geo} = 0.097\,W\,m^{-2}$. In the deep hypolimnion, the vertical diffusivity increases gradually from 0.3 to 1 $cm^2\,s^{-1}$ towards the lake bottom (Fig. 6). Analogously, the vertical diffusivity is related to the turbulent flux of dissolved solids, F_{sed}^{tD}, by

$$K_d = -\frac{F_{sed}^{tD}}{\varrho \gamma_s \partial \kappa_{20}/\partial z} \qquad [m^2\,s^{-1}] \tag{10}$$

Combining Eqs. (7), (9) and (10) we can estimate the steady turbulent flux of dissolved solids by

$$F_{sed}^{tD} = \frac{\gamma_s \partial \kappa_{20}/\partial z}{c_p \partial T/\partial z} F_{geo} = \frac{\alpha \gamma_s}{c_p \gamma_\varrho} R_\varrho F_{geo} \approx 3.1 \cdot 10^{-9}\,kg\,m^{-2}\,s^{-1} \tag{11}$$

This turbulent upward mass flux from the deep water is in reasonable balance with the vertical particle flux induced by primary production. If we represent the composition of the algal biomass stoichiometrically by the simple formula CH_2O, the upward mass flux from the deep water, given by Eq. (11), would correspond to 11% of the primary production in the epilimnion, which is reported to be

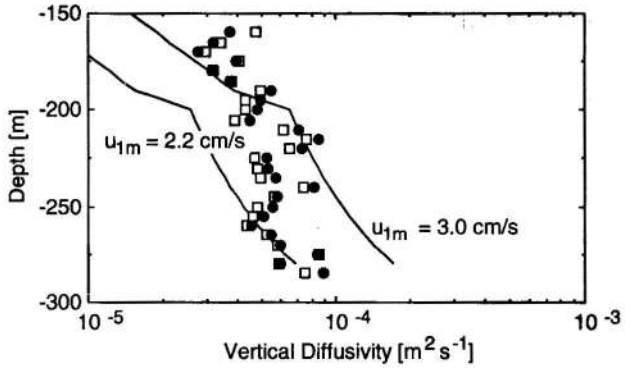

Figure 6. Vertical eddy diffusivity estimated from Eqs. (9) and (10) for stationary vertical fluxes of heat $F_{geo} \approx 0.097\ \mathrm{W\,m^{-2}}$ (black dots), and of dissolved solids $F_{sed}^{tD} = 3.1 \cdot 10^{-9}\ \mathrm{kg\,m^{-2}\,s^{-1}}$ (white squares). The lines correspond to vertical mixing rates calculated from bottom currents of 2.2 and 3.0 $\mathrm{cm\,s^{-1}}$ (Wüest et al., 1990). Above 200 m depth, the effect of mixing in the interior of the water column obviously exceeds that of boundary mixing

0.35 kg $\mathrm{C\,m^{-2}\,yr^{-1}}$ (Polli and Simona, this issue). If we include calcite, which also undergoes dissolution, and consequently also contributes to the upward mass flux, the fraction of mineralized algae in the deep water would still correspond to 9% of primary production, a value which is typical for deep lakes (Gächter, pers. communication). We conclude that the vertical diffusivities given by Eq. (9) (Fig. 6) are consistent with the geochemical gradients observed in the deep water layers.

If vertical mixing, however, were due to the completely different process of double diffusion, the ratio between the fluxes of heat and dissolved solids would be different. As explained in Fig. 4, heat is transported more efficiently than dissolved solids. Laboratory experiments show that, for $R_\varrho > 2$, the density flux due to salinity is only 15% of the density flux due to heat (Turner, 1973). If we apply this result to our deep water situation, using Eqs. (7) and (11) the mass flux due to double diffusion (index dD) would be

$$F_{sed}^{dD} \approx 0.15\,\frac{\alpha\gamma_s}{c_p\gamma_\varrho}\,F_{geo} = \frac{0.15}{R_\varrho}\,F_{sed}^{tD} \approx \frac{1}{30}\,F_{sed}^{tD}, \qquad [\mathrm{kg\,m^{-2}\,s^{-1}}] \tag{12}$$

which amounts to only one thirtieth of the flux of dissolved solids determined by Eq. (11). Even if we allow a large error for the turbulent F_{sed}^{tD} in Eq. (11), we can conclude that fluxes due to double diffusion are far smaller than those due to shear-induced turbulence.

b) Bottom boundary mixing

This last conclusion implies that shear instabilities are the dominant mixing mechanism in the deep water. However, the vertical gradients of the horizontal velocity profile $u(z)$ of the internal seiches, $\partial u/\partial z$, are small in the interior water body

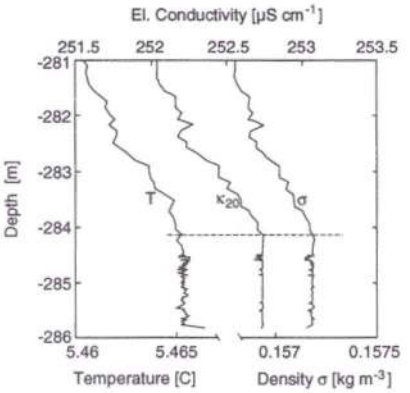

Fig. 7. An example of a completely homogenized bottom layer (mid-lake profile). Fluctuations T' and κ'_{20} are extremely small: $T' < 0.4\,\text{mK}$ and $\kappa'_{20} < 0.04\,\mu\text{S cm}^{-1}$

(except close to the sediment) and can, therefore, hardly be responsible for inducing instabilities (Münnich et al., 1992). High frequency internal waves, another path for turbulence, are strongly damped in the deep water layers, as the shortest possible period of such waves, given by $T_{\min} = 2\pi \cdot N^{-1}$, is about 2 hours for the *in situ* stability of $N^2 \gtrsim 10^{-6}\,\text{s}^{-2}$. Therefore, we do not expect the internal deep water body (away from the bottom boundary) to undergo intensive turbulence.

The zone of highest shear is rather close to the sediment, because currents, generated mainly by barotropic and baroclinic waves, vanish at the sediment-water interface. As a consequence, turbulent kinetic energy is produced by the shearing motion of the bottom current and mixing close to the sediment undergoes subsequent intensification. Figure 7 shows such an example of a well mixed bottom layer, which can be produced by current speeds as low as 1 cm/s (Wüest et al., 1990).

The question arises whether typical bottom currents occurring in the basin can explain the relatively large vertical diffusivities shown in Fig. 6. To test for consistency, we applied a bottom mixing model based on simple assumptions (Garrett, 1990, Eq. (2) in his paper). We assumed in particular that the dissipation of turbulent kinetic energy by bottom friction (described by a drag coefficient of $1.5 \cdot 10^{-3}$) occurs within a 10 m thick bottom layer and that 10% of this energy is stored as potential energy by mixing (Wüest et al., 1990). In Figure 6, the vertical diffusivity profiles calculated by this model for bottom currents of $u_{1\text{m}} = 2.2\,\text{cm s}^{-1}$ and $u_{1\text{m}} = 3.0\,\text{cm s}^{-1}$ (1 m above bottom), are compared to the steady-state diffusivity of Eq. (9). This comparison reveals that, although the profile shapes do not match perfectly, a mean bottom current of $u_{1\text{m}} \approx 2.6\,\text{cm s}^{-1}$ would provide the required energy for mixing. In fact bottom currents measured during February–March 1990 in the centre of the northern basin were found to vary within the range of 1 to $3.5\,\text{cm s}^{-1}$ (Salvadè et al., this issue). Since the simultaneously measured wind velocities do not deviate significantly from the long-term mean (LSA, 1989), we can conclude that the wind energy input is sufficient to achieve the observed mixing rates in the long term.

5. Conclusions relevant to primary productivity

Based on the tritium-helium distribution presented here and the temporally constant chemical profiles discussed by Barbieri and Mosello (this issue), it can be concluded that the deep water in the northern basin has not experienced deep convection for several decades. The 1960s saw not only an increase in phosphorous concentration, and consequently in primary productivity and calcite precipitation, but also complete oxygen depletion in the deep water (Barbieri and Mosello, this issue). It is not possible to determine by an oxygen balance whether the previous oxic conditions were due to the absence of stratification or were the result of low oxygen consumption due to low productivity. Today, however, due to the suppression of vertical mixing by the biogenically dependent upward ion flux, most of the hypolimnion is permanently stratified.

Will this stratification disappear if primary productivity is reduced? Since the geothermal heat flux acts to destabilize the deep water, we can expect a reduction in primary productivity to result in a decrease in the geochemical gradients even if wind activity is low. An analysis of the ratio of the density gradients (Fig. 3) reveals that, in order to prevent long-term biogenic density stratification in the deep water, the ion flux from the deep water and, consequently, primary productivity, would have to be reduced by a factor of four to five (at the present bottom temperature). In agreement with this hypothesis, Niessen et al. (this issue) has estimated that, prior to the onset ($\sim$ 1930) of the recent eutrophication, primary productivity was about a fifth of its present level.

ACKNOWLEDGEMENTS

We are grateful to D. M. Imboden for helpful discussions, V. Graf and H. Bolliger for the typing and drawing work, C. Dinkel for the ion measurements, M. Simona for piloting and providing the ship and D. M. Livingstone for improving the English. The constructive criticism of two anonymous reviewers helped to improve the manuscript. This work was supported by Swiss National Science Foundation grant 20-27751.89.

Appendix

Dissolved solids and total electrical conductivity (data from 16. 5. 1990)

	HCO_3^-	SO_4^{-2}	Cl^-	Ca^{2+}	Mg^{2+}	Na^+	K^+	NH_4^+	$\kappa_{20}^{\text{in situ}}$ (1)	$\kappa_{20}^{\text{calculated}}$ (2)	Salinity
Depth [m]	Concentration [10^{-3} val/l]								[$\mu S\,cm^{-1}$]	[$\mu S\,cm^{-1}$]	[‰]
50	2.330	0.284	0.051	1.652	0.721	0.074	0.034	0	[illegible]	227.6	0.202
180	2.642	0.222	0.049	1.911	0.749	0.095	0.039	0.022	[illegible]	250.9	0.225
266	2.710	0.190	0.050	1.934	0.767	0.088	0.040	0.059	[illegible]	255.2	0.228
	Equivalent conductance λ_{20}^{∞} at $T = 20\,°C$ and infinite dilution [$mS\,cm^{-1}\,(val/l)^{-1}$] (Schwabe, 1986)										
	40.28	71.66	68.88	53.21	47.11	44.92	66.58	66.58			
	Reduction coefficient f_i [−] (3)										
	0.95	0.90	0.96	0.90	0.90	0.95	0.96	0.95			

(1) Determined by the approximation $\kappa_{20} = f(T) \cdot \kappa_T$, where $f(T)$ is a empirical relation due to values from (Schwabe, 1986)
(2) The deviation of about ~ 1.6% between calculated (Eq. (3)) and in situ conductivity is comparable to the accuracy of the chemical analysis
(3) Determined by using data from Handbook of Chemistry and Physics

REFERENCES

Bührer, H. and H. Ambühl, 1975, Die Einleitung von gereinigtem Abwasser in Seen. Schweiz. Z. Hydrol. 37:347–369.

Finckh, P., 1981, Heat-flow measurements in 17 perialpine lakes: Summary. Geological Society of America. Bulletin, part I, 92:108–111.

Garrett, C., 1990, The Role of Secondary Circulation in Boundary Mixing. J. Geophys. Res. 95:3181–3188.

Huppert, H. E. and J. S. Turner, 1972, Double-diffusive convection and its implications for the temperature and salinity structure of the ocean and Lake Vanda. J. Phys. Oceanogr. 2:456–461.

Joller, T., 1985, Untersuchung vertikaler Mischungsprozesse mit chemisch-physikalischen Tracern im Hypolimnion des eutrophen Baldeggersees. Dissertation ETH, Nr. 7830, 94 pp.

Karagounis, I., 1992, Ein physikalisch-biochemisches Seemodell: Anwendung auf das Nordbecken des Luganersees. Mitteilungen VAW Nr. 116 (Dissertation ETH, 156 pp.).

KUeR, 1991, 30. Bericht der eidg. Kommission zur Überwachung der Radioaktivität. BAG, Bern.

LSA, Laboratorio Studi Ambientali, 1989, Ricerche sull'evoluzione del Lago di Lugano; aspetti limnologici. Programma quinquennale 1983–1987; Ed.: Commissione Internazionale per la Protezione delle Acque Italo-Svizzere.

LSA, Laboratorio Studi Ambientali, 1990, Ricerche sull'evoluzione del Lago di Lugano; Ed.: Commissione Internazionale per la Protezione delle Acque Italo-Svizzere.

Münnich, M., A. Wüest and D. M. Imboden, 1992, Observations of the second vertical mode of the internal seiche in an alpine lake (Limn. Oceanogr., in press).

Newman, F. C., 1976, Temperature steps in Lake Kivu: a bottom heated saline lake. J. Phys. Oceanogr. 6:157–163.

Padman, L. and T. M. Dilon, 1987, Vertical heat fluxes through the Beaufort Sea thermohaline staircase. J. Geophys. Res. 92:10799–10806.

Schwabe, K., 1986, Physikalische Chemie, Band 2: Elektrochemie Akademie-Verlag, Berlin, 443 pp.

Stumm, W. and J. Morgan, 1981. Aquatic Chemistry. Wiley Interscience, New York, 780 pp.

Torgersen, T., W. B. Clarke and W. J. Jenkins, 1979, The tritium/helium-3 method in hydrology, IAEA-SM-228/49, pp. 917–930.

Turner, J. S., 1973, Buoyancy Effects in Fluids. Cambridge University Press, 370 pp.

Ulrich, M., 1991, Modeling of Chemicals in Lakes – Development and Application of User-Friendly Simulation Software (MASAS and CHEMSEE) on Personal Computers, Dissertation ETH, Nr. 9632, 213 pp.

Weiss, W. and W. Roether, 1980, The rates of tritium input to the world oceans. Earth Planet. Sci. Lett. 49:435–446.

Wüest, A., W. Aeschbach, M. Hofer, R. Kipfer und M. Schurter, 1990, Dichtestruktur und Alter hypolimnischen Tiefenwassers im Luganersee-Nordbecken. Proc. International Symposium: Limnological Aspects and Management of the Lake of Lugano, Lugano, Nov. 5–7.

Received 14 February 1992;
revised manuscript accepted 8 July 1992.